Eur. Phys. J. D **16**, 103–106 (2001)

THE EUROPEAN PHYSICAL JOURNAL D

EDP Sciences

Large-scale molecular dynamics simulations of high energy cluster impact on diamond surface

Y. Yamaguchi[a] and J. Gspann

Institut für Mikrostrukturtechnik, Forschungszentrum Karlsruhe and Universität Karlsruhe, Postfach 3640, D-76021 Karlsruhe, Germany

Received 22 November 2000

Abstract. Large-scale molecular dynamics simulations with high acceleration energy on a diamond surface were performed in order to investigate the surface erosion process. Accelerated argon or CO_2 clusters (∼960 atoms, 100 keV/cluster) impacted on the (111) surface of diamond which consisted of more than 1,000,000 carbon atoms. A typical hemispherical crater appeared about 0.7 ps after the impact, and two or three-layered shockwaves were formed and propagated to certain directions, but the crater was immediately filled up with the fluidized hot carbon material due to the collective elastic recovery before the reflection of the shockwave. The impact energy of the cluster was at first transferred mainly as kinetic energy of the diamond surface in a short time, and the potential energy was activated later. The activated carbon and oxygen atoms from the impact cluster stimulated the evaporation from the diamond surface for the CO_2 cluster impact while the evaporation seemed to be suppressed by the argon atoms themselves for the argon cluster impact.

PACS. 36.40.-c Atomic and molecular clusters – 31.15.Qg Molecular dynamics and other numerical methods

1 Introduction

Atomic or molecular cluster beams are one of the most useful tools for surface modification including deposition, ion implantation and chemical and physical erosion, and ion cluster beam (ICB) deposition for thin film growth has especially long been studied and discussed [1]. The authors' group succeeded to generate intense beams of neutral clusters from pure vapor expansions of cesium, zinc, silver and, for periods of minutes, gallium by using feed vapor pressures in the range of bar [2]. However, broad beam ionization and acceleration of such high-intensity metal beams is still required in order to fully achieve the original ICB deposition concept.

On the other hand, gas cluster beams can easily be obtained from high-density source gas conditions [3], as long and deeply investigated for nuclear fusion purposes [4]. The authors' group has applied higher accelerated ionized cluster beams as the erosion source of nano- and micro-scale surface structuring [5]. In this technique, clusters consisting of about 1000 CO_2 molecules are accelerated to 100 keV. The impact-induced high energy density creates reactive plasma of cluster and surface material, and therefore, the technique is called RACE (reactive accelerated cluster erosion). With continuous impacts, very smooth eroded surfaces were obtained for diamond, silicon and glass. In addition, hillocks were induced by single impacts instead of craters which were expected from the macroscopic impact experiments [6]. These results seemed to be ascribed to the fluidization of the surface material.

In this paper, molecular dynamics (MD) simulations of cluster impacts on a diamond surface are performed. MD studies on cluster impact have been reported such as argon cluster on sodium chloride with 1 keV/cluster [7], or copper cluster on copper with up to 10 keV/cluster [8]. In this study, large-scale MD simulations with highly accelerated clusters of 100 keV/cluster are performed in order to investigate the surface erosion process, and the differences between inert argon and reactive CO_2 cluster impacts are also discussed.

2 Method

2.1 Potential functions

The empirical potential function proposed by Brenner with the parameters in potential I is applied for the interaction among carbon atoms [9]. The conjugate-compensation term F in his original expression is ignored here [10]

$$E_b = V_R + V_A \tag{1}$$

$$V_R = f(r_{ij})\frac{D_e}{S-1}\exp\{-\beta\sqrt{2S}(r_{ij}-R_e)\} \tag{2}$$

[a] e-mail: yaya@photon.t.u-tokyo.ac.jp

Table 1. Potential parameters for oxygen related interactions.

	D_e (eV)	S	β (1/Å)	R_e (Å)
C-O	12.04	1.11	2.3	1.1
O-O	14.92	1.056	3.043	0.9665

a_1	b_1	c_1	d_1	g_0
0.0777	0.13415	1.6733	0.0171	1.0728

Table 2. Lennard-Jones potential parameters.

$\sigma_{\text{Ar-C}}$ (Å)	$\sigma_{\text{Ar-Ar}}$ (Å)	$\varepsilon_{\text{Ar-C}}$ (J)	$\varepsilon_{\text{Ar-Ar}}$ (J)
3.385	3.4	8.013×10^{-22}	16.7×10^{-22}

$$V_A = -B^* f(r_{ij}) \frac{D_e S}{S-1} \exp\{-\beta\sqrt{2/S}(r_{ij} - R_e)\} \quad (3)$$

$$B^* = \frac{B_{ij} + B_{ji}}{2}, B_{ij} = [1 + \sum_{k(\neq i,j)} G_c(\theta_{ijk}) f(r_{ik})]^{-\delta} \quad (4)$$

$$G_c(\theta) = a_0 \left(1 + \frac{c_0^2}{d_0^2} - \frac{c_0^2}{d_0^2 + (1+\cos\theta)^2}\right) \quad (5)$$

where r_{ij}, V_R, V_A and $f(r)$ denote the distance between carbon atoms i and j, Morse-type repulsive and attractive terms and cut-off function, respectively.

The interaction potential of C-O and O-O were derived from the Brenner's equation in the following manner. Assuming that an oxygen atom has initially additional two fixed virtual bonds (ks in eq. (4)) that are automatically located at the optimum positions for real bonds. Thus, the functions B_{ij} in eq. (4) and $G(\theta)$ in eq. (5) are expressed as follows.

$$B_{ij(i:\text{oxygen})} = [g_0 + \sum_{k(\neq i,j)} G_o(\theta_{ijk}) f(r_{ik})]^{-\delta} \quad (6)$$

$$G_o(\theta) = a_1 \cos\theta + \frac{b_1}{c_1 + \cos\theta} + d_1. \quad (7)$$

Eq. (7) was fitted as a function of the bond angle. Then the Morse parameters D_e, S and β were defined from the normal C-O and O-O binding energy data. These parameters are shown in Table 1.

The Lennard-Jones potential is applied for carbon-argon and argon-argon interactions with the parameters in Table 2.

2.2 Initial and boundary conditions

The impact target must be large enough in order to avoid the side effect mainly due to the impact-induced shockwave. The impact target of diamond (111) surface consists of a hexagonal internal full-simulated region and a surrounding external region. Considering that the effect of the external region far from the impact point is not crucial to the impact phenomena, only 1/6 of the external region is simulated, and its mirror and rotated images are connected with the internal region in order to reduce the calculation time. The internal and external regions contain 758,440 and 308,240 carbon atoms, respectively (2,584,741 carbon atoms including virtual images). The vertical depth and the length of the diagonal line of the internal region are about 115 Å and 122 Å respectively, and the external region extends by another 50% of the symmetric region in each direction. The outer boundary of the external region is fixed and the temperature is controlled at 300 K near the outer boundary with the Langevin method. The whole system was preliminary relaxed at 300 K before the impact.

The impact clusters were obtained by cooling the liquid phase argon or CO_2 to 40 K, and these clusters contain 961 atoms for argon and 960 molecules for CO_2 referring our experimental data [5]. The Lennard-Jones potential was also applied only for the inter-CO_2 interactions here, but it is not applied for the impact simulation.

Verlet's method was adopted to integrate the equation of motion with the time step dt of 0.2 fs for the first 2 ps and 0.5 fs afterwards.

3 Results and discussions

3.1 Argon cluster impact

Fig. 1 shows snapshots of the argon cluster impact simulation with the acceleration energy of 100 keV, where a 10 Å sliced view parallel to the impact direction is shown, and atoms with larger velocity have darker color. A typical hemispherical crater appears about 0.7 ps after the impact, and two or three-layered flat shockwaves propagate to $(\bar{1}\bar{1}\bar{1})$, $(1\bar{1}\bar{1})$, $(\bar{1}1\bar{1})$ and $(\bar{1}\bar{1}1)$ directions [Fig. 1(b)]. However, the crater is immediately filled up with the fluidized hot carbon material around the impact point due to elastic recovery before the reflected shockwave comes back from the end boundary [Fig. 1(c, d)]. The shockwave goes through the impact point at about 3.0 ps and the surface is mounded up, but no significant side effect can be seen because the impact point is still hot and is not recrystallized yet [Fig. 1(e)]. The velocity of the shockwave is about 14-15 km/s, a little slower than 18 km/s in diamond. The size of the transient crater is about 60 Å in diameter and that corresponds well to the size expected from macroscopic ballistic experiment [6].

Fig. 2 shows the energy profile of the system for the first 1.5 ps, where E_k and E_p denote the kinetic and potential energy as the offset from the initial values, and suffixes Ar, int and ext are for argon, carbons atoms in the full-simulated and symmetric regions, respectively. The impact energy is at first transferred mainly to the kinetic energy E_k^{int} until about 0.3 ps, and then, the potential energy E_p^{int} gradually increases. E_p^{int} has a maximum at about 0.7 ps when the crater size becomes almost the largest, and that time is long before the reflection of the shockwave. Therefore, it is clear that the crater is filled up not due to the shockwave, but due to the local elastic recovery. At about 0.8 ps, the shockwave propagates out of the internal region and kinetic and potential energies

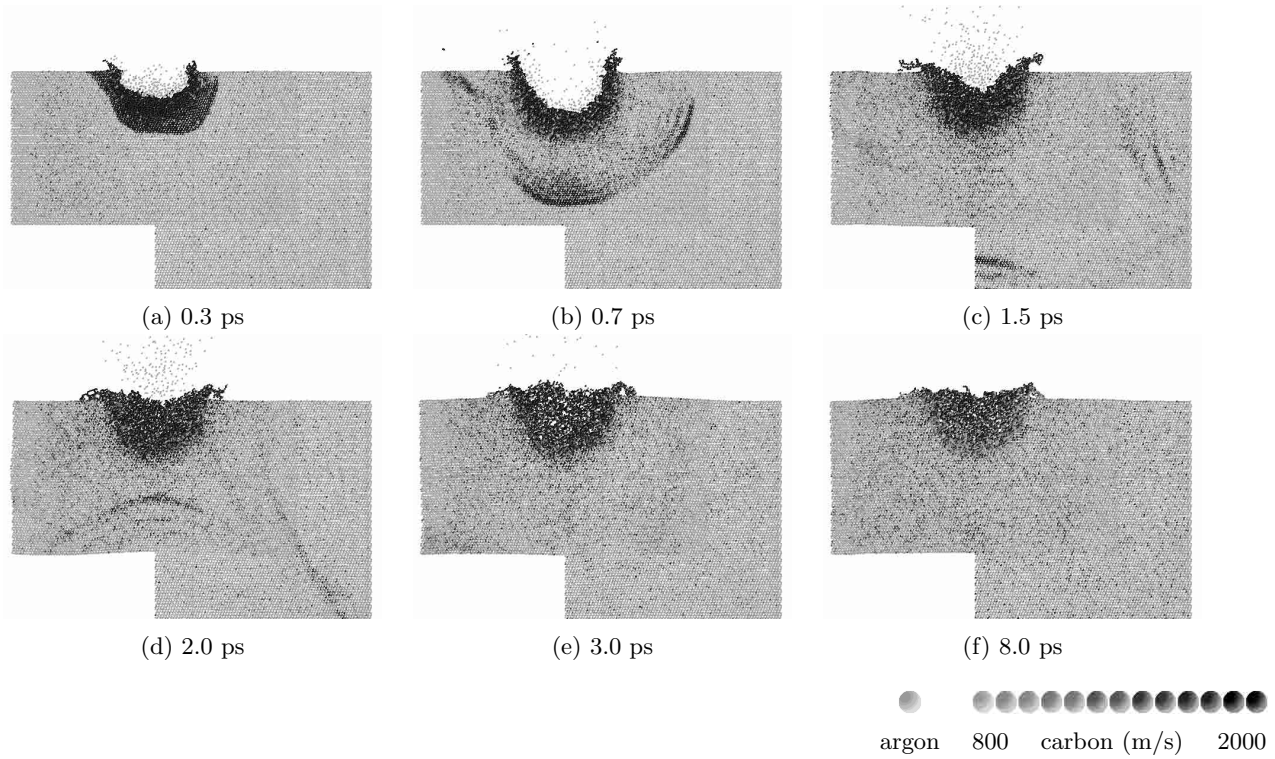

Fig. 1. Snapshots of argon cluster impact simulation (sliced view).

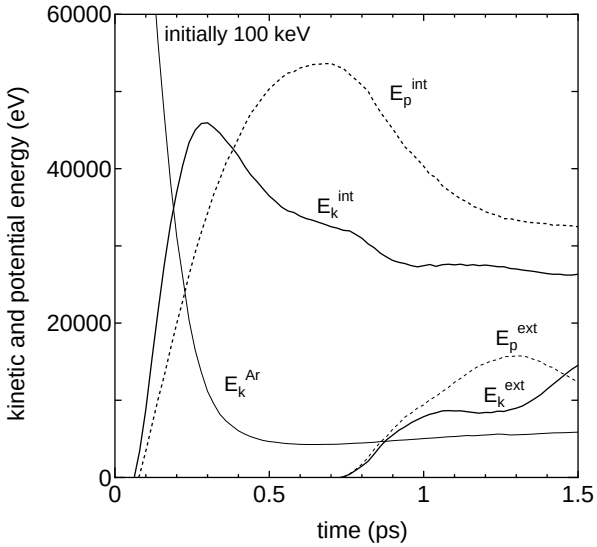

Fig. 2. Kinetic and potential energy profiles.

of the external region are excited, and then, the shock reflects at the end boundary at about 1.3 ps. About 94% of the 100 keV initial impact energy is transferred into the target, and the impact itself is obviously ascribed to be an inelastic process.

3.2 Comparison of argon and CO_2 cluster impacts

Fig. 3 shows a comparison of the enlarged snapshots of the argon and CO_2 cluster impact simulations. No significant difference can be seen in the structures of craters at 0.7 ps [Fig. 3(a1, b1)] because the primary impact stage is simply a hard collision process. Therefore, the structures and velocities of the shockwaves are also almost the same. The difference appears in the collective motion of the surface after the impact. For the argon cluster impact, the evaporation of carbon atoms from the surface is strongly suppressed in the vertical direction by the argon atoms themselves as shown in Fig. 3(a2, a3), and carbon atoms can escape only from the edge of the impact point. Thus, the impact surface is rather smooth. On the other hand, the activated carbon and oxygen atoms stimulate the evaporation by taking carbon atoms away from the surface for the CO_2 impact as shown in Fig. 3(b2, b3). The numbers of carbon atoms out of the diamond surface ($N_{\mathrm{C}}^{\mathrm{out}}$) for both impacts are shown in Fig. 4, where the number is defined as the offset from the initial condition. The number of oxygen atoms staying on the diamond surface ($N_{\mathrm{O}}^{\mathrm{in}}$) is also shown for CO_2 impact. The number of carbon atoms escaped from the surface for CO_2 impact is more than three times larger than that of argon impact, and that corresponds well to our experimental results [11]. It is also notable that not a few number of oxygen atoms stay on the surface after the impact.

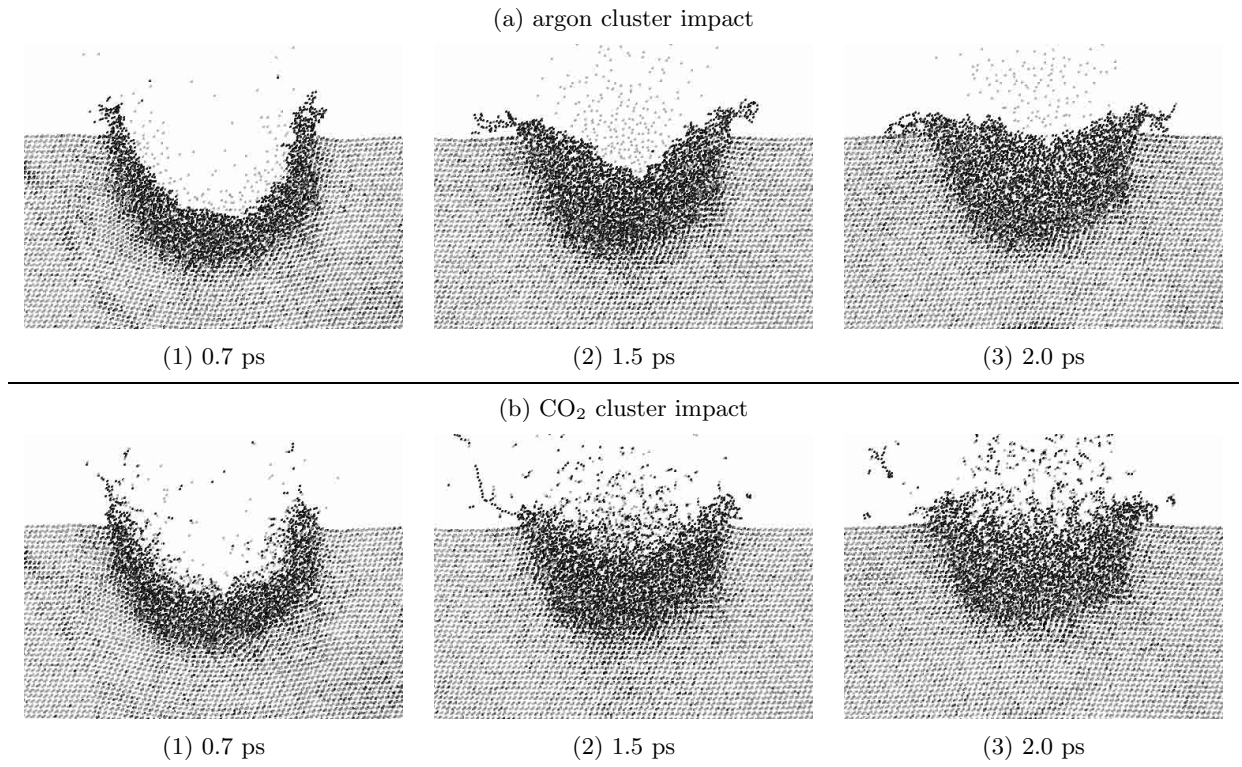

Fig. 3. Comparison of argon and CO_2 cluster impacts (sliced view, enlarged).

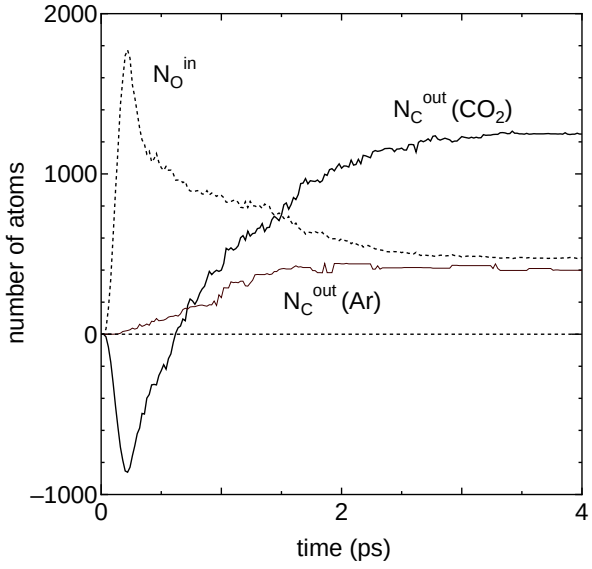

Fig. 4. Number of evaporating carbon atoms, and oxygen atoms remaining on the diamond surface.

4 Concluding remarks

Large-scale molecular dynamics simulations with high acceleration energy on a diamond surface were performed in order to investigate the surface erosion process. A hemispherical crater and two or three-layered shockwaves were once created after the impact, but the crater was immediately filled up with the fluidized hot carbon material due to elastic recovery. Compared to the argon cluster impact, the CO_2 cluster impact induced significant evaporation from the surface with the activated carbon and oxygen atoms from the cluster.

This work was supported by Grant-in-Aid for JSPS Fellows (No. 11-08826) from the Ministry of Education, Science, Sports and Culture, Japan.

References

1. J. Gspann, *Similarities and Differences between Atomic Nuclei and Clusters* (The American Institute of Physics, New York, 1998), p. 299.
2. J. Gspann, Trans. Mat. Res. Soc. Jap. **17**, 107 (1994).
3. E.W. Becker, K. Bier, W. Henkes, Z. Phys. **146**, 333 (1956).
4. E.W. Becker, Laser Part. Beams **7**, 743 (1989).
5. A. Gruber, J. Gspann, H. Hoffmann, Appl. Phys. A **68**, 197 (1999).
6. J. Gspann, *From Cluster to Crystals* (Kluwer, Amsterdam, 1992), p. 463.
7. C.L. Cleveland, U. Landman, Science **257**, 355 (1992).
8. M. Moseler *et al.*, Nucl. Inst. Meth. Phys. Res. B **164-165**, 522 (2000).
9. D.W. Brenner, Phys. Rev. B **42**, 9458 (1992).
10. Y. Yamaguchi, S. Maruyama, Chem. Phys. Lett. **286**, 336 (1998).
11. C. Becker, J. Gspann, R. Krämer, Eur. Phys. J. D **16**, 301 (2001).